Int. J. Nanosci. Nanotechnol., Vol. 18, No. 2, June 2022, pp. 143-156

Short Communication

Magneto Effects on Fe_3O_4 Nanoparticles through the Triangular and Rectangular Baffles on Thread Stretching Surface for Rotary Seals in Computer Hardware

Mohammad Mohsen Peiravi[1,*] and Arman Ashabi[2]

[1]Department of Mechanical Engineering, Technical and Vocational University (TVU), Tehran, Iran
[2]UM Power Energy Dedicated Advanced Centre (UMPEDAC), University of Malaya, Kuala Lumpur, Malaysia

(*) Corresponding author: Mohsenpeiravi@gmail.com
(Received: 4 September 2021 and Accepted: 12 December 2021)

Abstract

In this paper, variation of temperature and velocity profiles and the angular velocity of the nanofluid flow through triangular and rectangular baffles are investigated in the existence of a uniform magnetic field. The innovation of this paper is the investigation of nanofluid parameters passing on the different baffles on the stretching surface using the Finite Element Method. According to the results of different cases, the maximum nanofluid velocity is observed in rectangular baffles. The fluid velocity for nanofluid on the rectangular baffles is 19.5% more than on other baffles. At X=0.2 to X=0.8 for rectangular baffles and triangular baffles, the average velocity of nanofluid flow in the rectangular baffles is equal to u=0.4 but, the average velocity of nanofluid flow in the triangular baffles is u=0.04. The maximum nanofluid temperature is observed in rectangular and triangular baffles. The temperature profiles of nanofluid on the rectangular and triangular baffles are 50% more than other baffles.

Keywords: *Finite element method, Magnetic effect, Nanofluid Effects, Rectangular baffles, Thread stretching sheet.*

Nomenclature

H	=	distance the plates (m)
C	=	Nano fluid concentration
σ	=	Electrical conductivity (s/m)
K	=	Dimensionless temperature
x, y	=	coordinates (m)
u, v	=	velocity components (m/s)
θ	=	Dimensionless temperature
ϑ	=	Kinematic viscosity (m^2/s)
C_p	=	Specific heat at constant pressure (j/kg.k)
k	=	Thermal conductivity (w/m.k)
P	=	Modified fluid pressure
g_y	=	gravitational acceleration (m/s^2)
$\emptyset$	=	Dimensionless concentration
Pr	=	Prandtl number (υ/α)

Nt = Thermo-phoretic parameter
Nb = Brownian motion
T_c = temperature of the cold wall (K)
α = thermal diffusivity (m^2/s)
β = thermal expansion (1/K)
ρ = density (kg/m^3)
μ = dynamic viscosity (kg/m. s)
υ = kinematic viscosity (m^2/s)
ΔT = temperature difference (K)

1. INTRODUCTION

Thread stretching sheet with Different baffles is investigated with the steady-state two-dimensional flow of a micropolar/ classical Ferrofluid was assumed. A ferrofluid is a form of fluid in which microparticles of iron, magnetite, or cobalt exist.

Ferrofluids are made-up of magnetic iron pieces suspended in oil, commonly kerosene, with a surfactant to prevent oleic acid. Ferrofluids are used in rotary seals for computer hardware and other rotating shaft motors.

There is the main challenge between the nanofluid and nano-scale flow, so the physical properties and dynamical behavior of nanochannel flows have been practical applications in physics, chemistry, medicine, and electronics [1-3]. The flows inside nano-scale pores are also important due to their highly beneficial drag and heat transfer properties.

Researchers [4] evaluated the impacts of different arrangements at three-dimensional fibers on polymer matrix composite thermal conductivity under heat flux boundary conditions. The results signified that nondimensional temperature field in a PMC with the arrangement of a fiber, triplet, and triangular perpendicular to heat flux had a greater rate than a PMC with the arrangement of fibers along the way heat flux.

Scientists [5] presented the significance of the Hall current and Joule heating impacts on a peristaltic flow of a Rabinowitz fluid through a tapered tube. Scholars [6] studied the significance of partial slips and temperature jumps on the heat and mass transfer of a boundary layer nanofluid flowing through a stretched or shrinking surface. Researchers [7] investigated a novel mathematical approach to the Kelvin Helmholtz instability (KHI) saturated in porous media with heat and mass transfer. Scientists [8] studied Hybrid conduction, convection, and radiation heat transfer simulation in a channel with a rectangular cylinder. Modeling fluid and temperature fields were used the lattice Boltzmann approach based on the D2Q9 scheme. In [9] scientists investigated that fins shape and arrangement effects on entropy generation and hybrid fluid-solid-fluid heat transfer in 3D multi-floors enclosure with heat flux boundary condition by lattice Boltzmann method (LBM). At Peiravi et al. [10] researched Nanoparticles distribution in multi-phase heat transfer between 3D cubical. The novelty of this paper is the simultaneous simulation of two separate multi-phase nanofluids in two 3D enclosures under a heat flux boundary condition.

Abbasi et al. In [11] the effects of slip and convective boundary conditions are considered in the heat and mass transfer of MHD stagnation point flow of water-based nanofluids. The numerical results show that the velocity at a point for the stretching sheet decreases as the values increase, whereas temperature and nanoparticle concentration increase as the velocity slip parameter increases.

Nanofluids are fluids containing Nano particle-sized fine particulate matter. Since these fluids have great heat transfer

potential, special attention has been paid to this group of fluids as heat transfer environments [12-15].

Scholars in [16] numerically investigated the buoyant convective flow and thermal transport enhancement of Cu–H2O Nanoliquid in a differentially heated upright annulus having a thin baffle. Scientists [17] examined features of double stratification on stagnation point flow of Walter's B Nanoliquid driven through Riga surface. Researchers [18] surveyed the impact of variable magnetic field and chemical reaction of MWCNT/Fe3O4–water hybrid nanofluid over an exponentially shrinking porous sheet with slip boundary conditions. Scholars [19] described the laminar flow of a Nanoliquid in a trapezoidal cavity, in addition to measuring convective exchanges that take place there.

Scientists [20] explored the comparative analysis of MoS2/C2H6O2 nanofluid and SiO2-MoS2/C2H6O2 hybrid nanofluid natural convective boundary layer flow through a stretching area. Researchers [21] investigated entropy generation of mixed convection for a lid-driven porous enclosure filled through a Nanoliquid and submitted to a uniform magnetic field.

In this paper, variation of temperature and velocity in the x-direction and the angular velocity of the nanofluid flow through triangular and rectangular baffles are investigated in the existence of a uniform magnetic field. The innovation of this paper is to investigate parameters of nanofluid flow passing from the different baffles on the stretching surface.

2. PROBLEM DEFINITION

On a stretching sheet with 12 numbers with Different baffles in the y > 0 direction, a steady-state two-dimensional flow of a micropolar/classical Ferrofluid is assumed in Fig.1. The triangular and rectangular baffles are used on the surfaces.

Fig. 1 shows the unsmooth boundary, which is very similar to the fractal solution theory [22,23]. The flow of nanofluid is entered with 20-degree temperature and angular velocity 0 from 4 directions and passes through the baffles and surface. The surface temperature is 30 degrees and the surface is stretched by (UW(x) = ax, a>0). The amount of velocity in the x-direction is 2m/s. In this article, the effect of the magnetic force is investigated on the surface.

The simulation time was about two hours using system performance; CPU core i3, RAM 4GB.

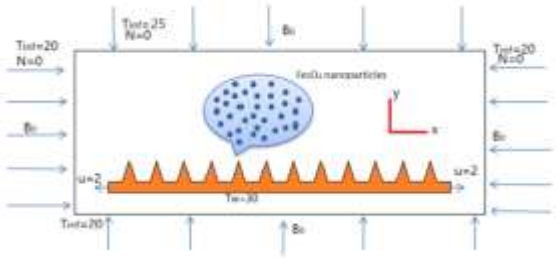

Figure 1. *Schematic of the threated stretching surface.*

Table 1: *Properties of water and Fe3O4 nanofluid at 20 degrees [24].*

	ρ(kg/m^3)	K(w/m.k)	C_p (j/kg.k)	σ
Fe_3O_4	5180	17.65	104	250
H_2O	997.1	0.613	4179	0.05

The finite element method is used to solve this article. Below, the governing equation for Ferrofluid is:

$$\frac{d}{dt}(\rho_{nf}) = \nabla.(\rho_{nf} v) \tag{1}$$

$$\rho_{nf}\left(\frac{dv}{dt}\right) = -\nabla_p + (2\mu_{nf} + \aleph)\nabla(\nabla.v) - (\mu_{nf} + \aleph)\nabla.(\nabla.v) + \aleph(\nabla.N) + j.B + \rho_{nf} g \tag{2}$$

$$\rho_{nf} j\left(\frac{dN}{dt}\right) = (\varphi + \lambda + Y_{nf})\nabla.(\rho_{nf}.N) - Y_{nf}\nabla.(\nabla.N) + \aleph(\nabla.v) - 2\aleph N + \rho_{nf} I \tag{3}$$

where effective density, effective dynamic viscosity, and spin gradient viscosity are presented by Brinkman [25], Bourantas, and Loukopoulos [26], respectively:

$$\rho_{nf} = (1-\varphi)\rho_f + \emptyset\rho_s \tag{4}$$

$$\mu_{nf} = \frac{\mu_f}{(1-\varphi)^{2.5}} \quad (5)$$

$$Y_{nf} = \left(\mu_{nf} + {\aleph}/{2}\right)j \quad (6)$$

In addition, flow is incompressible in the absence of external forces. Therefore, equations will be difficult to solve.

$$\rho_{nf}\left(\frac{dv}{dt} + (v.\nabla)v\right) = \left(\mu_{nf} + \aleph\right)\nabla^2 v + \aleph(\nabla.N) + j.B \quad (7)$$

$$\rho_{nf} j\left(\frac{dN}{dt} + (N.\nabla)N\right) = Y_{nf}.\nabla^2 N + \aleph(\nabla.v) - 2\aleph N \quad (8)$$

and the body force is proposed as follows:

$$j.B = -\sigma_{nf} B_0^2 v \quad (9)$$

The Ferrofluid electric conductivity represents as:

$$\sigma_{nf} = \left[1 + \frac{3(\sigma-1)\emptyset}{(\sigma+2) - (\sigma-1)\emptyset}\right]\sigma_f \quad (10)$$

and the governing equations go to:

$$\rho_{nf}\left(u\frac{du}{dx} + v\frac{du}{dy}\right) = \left(\mu_{nf} + \aleph\right)\frac{d^2u}{dy^2} + \aleph\frac{dN}{dy} - \sigma_{nf}B_0^2 u \quad (11)$$

$$\rho_{nf} j\left(u\frac{dN}{dx} + v\frac{dN}{dy}\right) = Y_{nf}\frac{d^2N}{dy^2} - \aleph\left(2N + \frac{du}{dy}\right) \quad (12)$$

The specific heat capacity and the effective thermal conductivity were researched by Din et al. [27].

$$\rho_{nf} C_{p,nf} = \rho_s C_{p,s} + (1-\emptyset)\left(\rho_f C_{p,f}\right) \quad (13)$$

$$\frac{k_{nf}}{k_f} = \frac{k_s + 2k_f - 2\emptyset\left(k_f - k_s\right)}{k_s + 2k_f + \emptyset\left(k_f - k_s\right)} \quad (14)$$

The energy equation is represented as follows:

$$u\frac{dT}{dx} + v\frac{dT}{dy} = \frac{k_{nf}}{C_{p,nf}}\frac{d^2T}{dy^2} - \frac{dq_r}{dy} \quad (15)$$

It is stated according to Rosseland's approximation as:

$$u\frac{dT}{dx} + v\frac{dT}{dy} = \frac{1}{C_{p,nf}}\left(k_{nf} + \frac{16\sigma^* T_\infty^3}{3k^*}\right)\frac{d^2T}{dy^2} \quad (16)$$

The boundary conditions are:

$$u = au_w(x),\ \ v = v_w,\ \ at\ \ y = 0, \quad u \leftrightarrow 0,\ \ y \to \infty \quad (17)$$

$$N = -\delta\frac{du}{dy}\ \ at\ \ y = 0, N \leftrightarrow 0,\ \ y \to \infty \quad (18)$$

$$T = T_w\,, at\ \ \ y = 0, \qquad T \leftrightarrow T_w,\ \ \ y \to \infty \quad (19)$$

The velocity components are called in the x and y directions u and v, respectively, to familiarize ourselves with these calculations. The suction and injection are represented by the positive and negative values of the surface mass transfer velocity, vw. The angular velocity is denoted by N. μ is dynamic viscosity, and δ is a constant in the 0-1 range. When set to 0, the microelement is specified. If δ=1/2, the concentration of microelements was shown to be weak. Furthermore, when the turbulent boundary layer flow is required, δ =1. j represents microelement inertia per unit mass, where is spin gradient viscosity. It is used similarity variables such as the following to make it easier to solve these nonlinear differential equations comfortably:

$$\eta = y\sqrt{\frac{a}{v_f}},\ \ u = axF'(\eta), v = -\sqrt{av_f}F(\eta), \quad N = ax\sqrt{\frac{a}{v_f}}G(\eta,\ \ \theta(\eta) = \frac{T - T_\infty}{T_w - T_\infty}, \quad (20)$$

By substituting the variables (20) into the Eq. (11), (12), (16):

$$\left(\frac{1}{(1-\emptyset)^{2.5}} + k\right)F'''(\eta) + \left(1 - \emptyset + \emptyset\frac{\rho_s}{\rho_f}\right)F(\eta)F''(\eta) - \left(1 - \emptyset + \emptyset\frac{\rho_s}{\rho_f}\right)F'^2(\eta) - M\left(1 + \frac{3(\sigma-1)\emptyset}{\sigma + 2 - (\sigma-1)\emptyset}\right)F'(\eta) + kG'(\eta) = 0 \quad (21)$$

$$\left(\frac{1}{(1-\emptyset)^{2.5}}+\frac{k}{2}\right)G''(\eta)+\left(1-\emptyset+\emptyset\frac{\rho_s}{\rho_f}\right)F(\eta)G'(\eta)-\left(1-\emptyset+\emptyset\frac{\rho_s}{\rho_f}\right)F'(\eta)G(\eta)-k\left(2G(\eta)+F''(\eta)\right)=0 \quad (22)$$

$$\frac{1}{Pr}\left(\frac{k_s+2k_f-2\emptyset\left(k_f-k_s\right)}{k_s+2k_f+\emptyset\left(k_f-k_s\right)}+R\right)\theta''(\eta)+\left(1-\emptyset+\frac{C_p)s}{C_p)f}\right)F(\eta)\theta'(\eta)=0 \quad (23)$$

and here are the new boundary conditions:

$$F(\eta)=S, F'(\eta)=\alpha, G(\eta)=-\delta F''(\eta), \theta(\eta)=1, \ at\ \eta=0 \quad (24)$$

$$F'(\eta)\leftrightarrow 0, G(\eta)\leftrightarrow 0, \theta(\eta)\to 0 \ \ at\ \ \eta\to\infty \quad (25)$$

3. SIMULATION METHODOLOGY

3.1. Finite Element Method (FEM)

The finite Element Method is an important numerical method that one of the practical applications for this method is FlexPDE software, that is solved the nonlinear partial differential equations and ordinary differential equations. FlexPDE is a builder of scripted finite elements and a numeric solver. In other words, from a script written by the user. FlexPDE carries out the necessary operation to transform a description of a partial differential equation system into a finite element model, Resolve the system, and graphical and tabular results. The present simulation used 200 mesh cells.

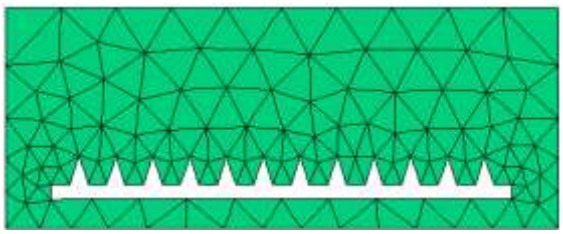

a) Triangular baffles near the bottom wall

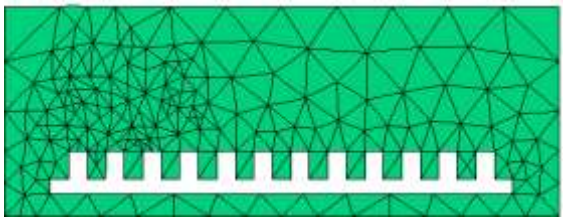

b) rectangular baffles near the bottom wall

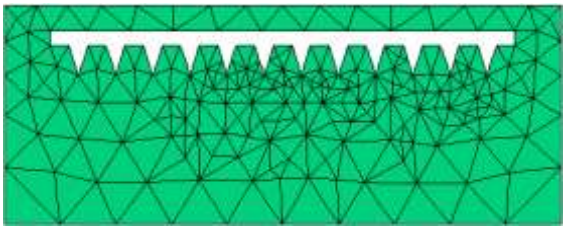

c) Inverse triangular baffles near the top

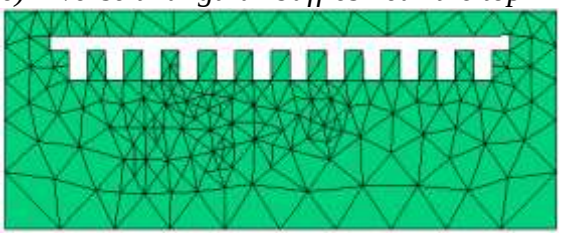

d) Inverse rectangular baffles near the top

Figure 2. *Comparison of mesh geometry for threated stretching surface.*

As it is clear, the largest grid of mesh is around the edges, because around the baffles the properties of Temperature and velocity of nanofluid flow change.

3.2. Validation of Method

In this section, for validation, we compare our work with Jalili et al. [24]. The amount of computational error in our work is very low compared to others. The maximum number of errors happened at η=1.5 and the minimum number of errors happened at η=1.

Table 1. *Comparison of temperature for present work and Jalili work [24] at K=10, δ=0.5, ϕ =0.03.*

	$\eta=1$	$\eta=1.5$	$\eta=2$	$\eta=2.5$
Present work	1.5	0.72	0.31	0.04
Jalili [9]	1.7	0.75	0.35	0.05

4. RESULT AND DISCUSSION

The effect of velocity changes in the x-direction around the baffles has more value than the surrounding space. According to fig. 3, the amount of flow velocity is reduced by increasing the distance from the surface in the y-direction. Furthermore, the rate of nanofluids is high, and the flow is balanced on both sides of the surface.

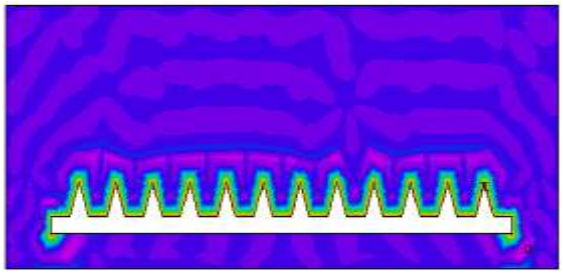

a) Triangular baffles near the bottom wall

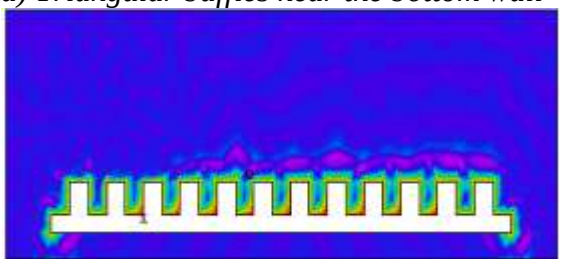

b) rectangular baffles near the bottom wall

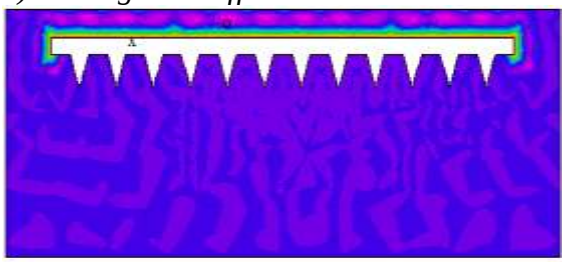

c) Inverse triangular baffles near the top

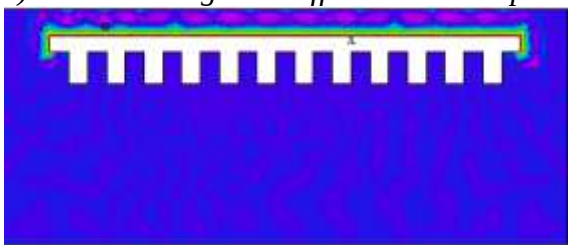

d) Inverse rectangular baffles near the top

Figure 3. *Comparison of velocity changes in the X direction in different baffles for threated stretching surface.*

Fig. 4 represented a variation of the angular velocity of the nanofluid flow through the surface. For the top baffles of the surface, the angular velocity values around that surface are very low, and the highest velocity values are observed at the end of the surface. According to Fig. 3, the angular velocity of nanofluid is very high around the baffles in the lower part of the surface, and the fluid flow particles orbit around the surface at high speeds. The fluid flow velocity is balanced in the entire space around the baffles.

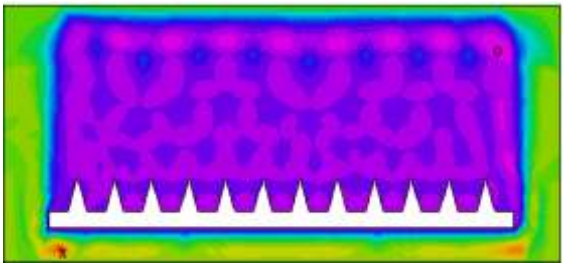

a) Triangular baffles near the bottom wall

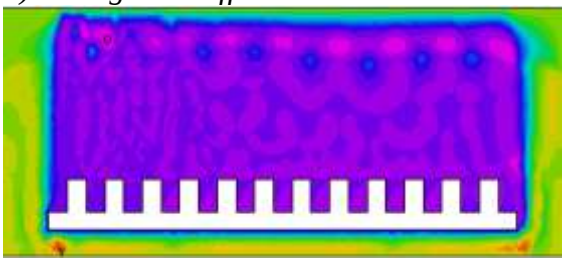

b) rectangular baffles near the bottom wall

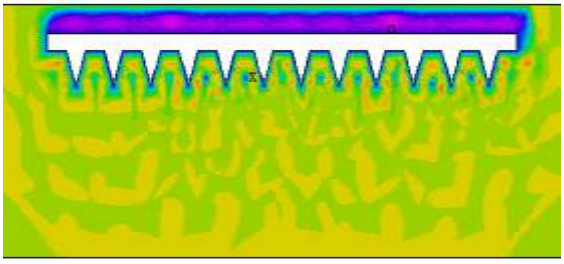

c) Inverse triangular baffles near the top

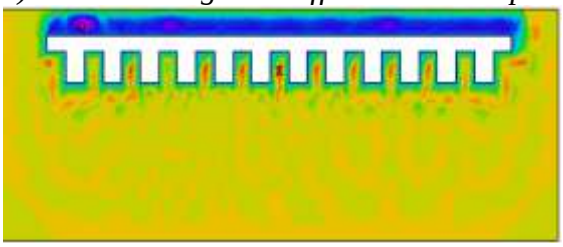

d) Inverse rectangular baffles near the top

Figure 4*. Comparison of angular velocity changes in different baffles for threated stretching surface.*

Fig. 5 shows the temperature changes of nanofluid around the surface and the baffles. According to figs. (a and b), the volume of nanofluid flow at the beginning of the surface and around the first baffle has reached its maximum. The fluid flow is decreased slightly, and the temperature is balanced around the other edges. At the end of the page, the temperature gets maximum. According to figs (c and d), the nanofluid temperature is very high around the baffles and by increasing the distance from the baffles, the amount of temperature is reduced.

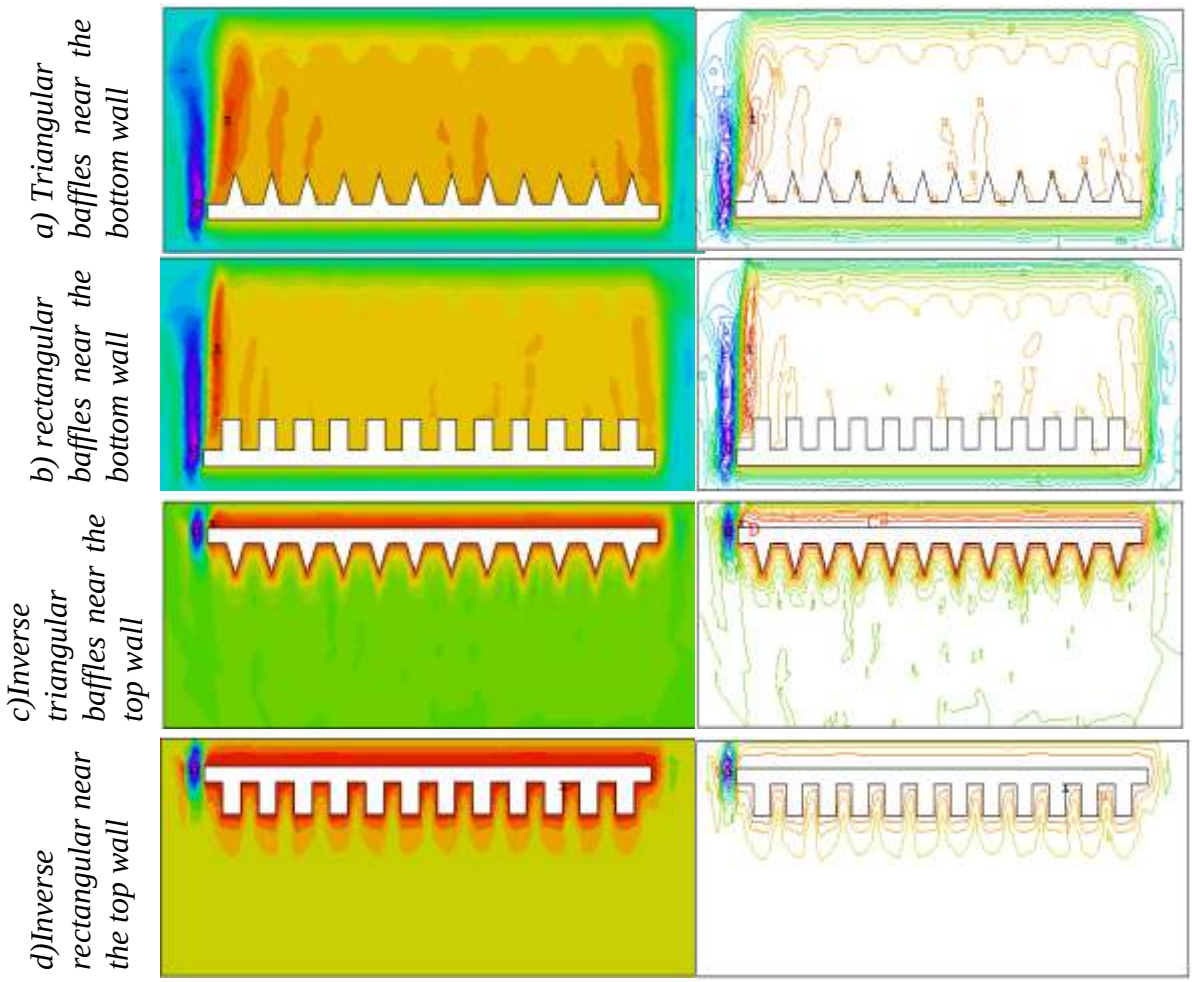

Figure 5. *Comparison of Temperature profiles for threated stretching surface with different baffles.*

For your convenience Fig. 6 clearly shows the temperature vector grid as a vector grid for the purpose of simplification and clarity. Because a slow-moving surface travels at a slow pace, the nanofluid temperature motion vectors surrounding it have low velocity and temperature.

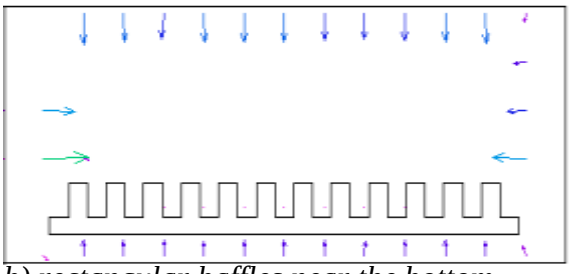

b) rectangular baffles near the bottom

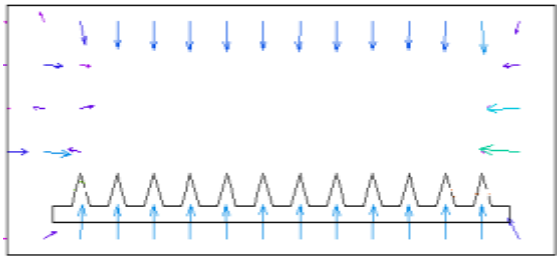

a) Triangular baffles near the bottom wall

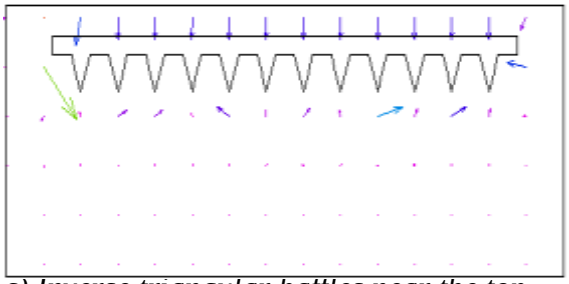

c) Inverse triangular baffles near the top

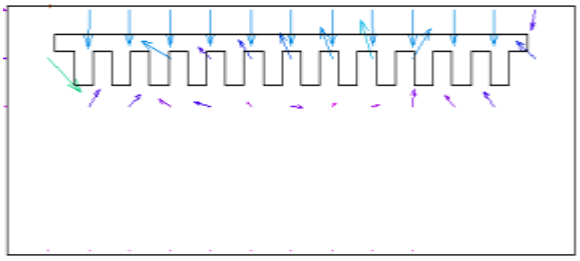

d) Inverse rectangular baffles near the top
Figure 6. *comparison of the vector grid Temperature changes in different baffles for threated stretching surface*

Aside from that, the increased concentration of vector grids of temperature surrounding the inverse rectangular baffles on the top wall results in an increase in the concentration of vector grids of temperature around the baffles. Because of this, these baffles have the ability to increase heat transfer to the surrounding environment.

The temperature of the nanofluid is decreased from a maximum of 35 degrees to 26 degrees in Fig. 7, which shows baffles in the rectangular and triangular shapes. The quantity of fluid temperature in figures a-7 and b-7 is minimal at the start of the simulations. Baffles are used to lower the temperature of the flow from 35 degrees to 25 degrees by passing nanofluid flow through them. Figures c-7 and d-7 show that the nanofluid temperature remains constant throughout the baffles. The temperature has been raised to 35 degrees .

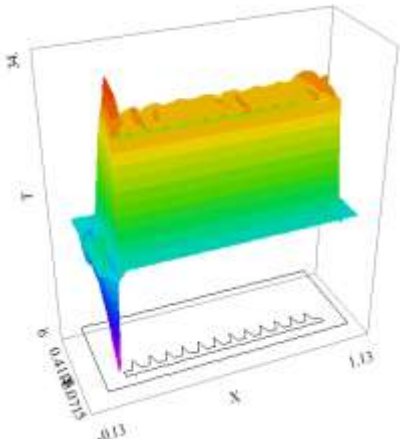

a) Triangular baffles near the bottom wall

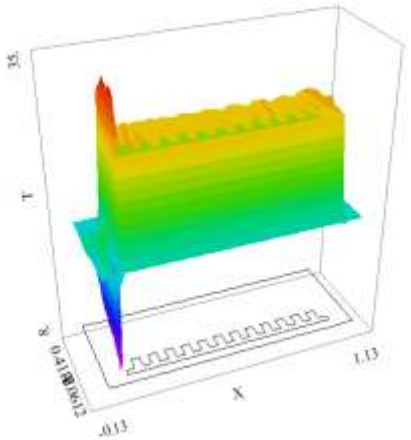

b) rectangular baffles near the bottom wall

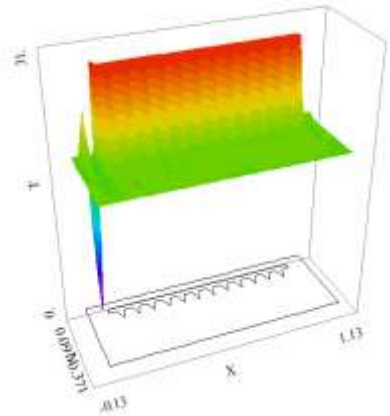

c) Inverse triangular baffles near the top

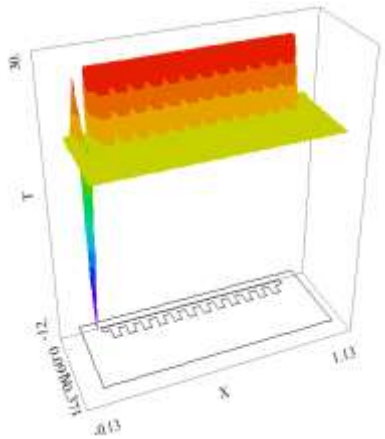

d) Inverse rectangular baffles near the top
Figure 7. *Comparison of the Temperature changes in different baffles for threated stretching surface.*

Figure 8 shows that the flow rate of nanofluid is initially low owing to the usage of rectangular and triangular baffles. However, after passing through the other baffles, the flow rate of nanofluid increases and ultimately reaches a value of 2 from a

value of 0. In combination with Figures a-8 and b-8, it can be shown that the nanofluid velocity rises in the direction of the y-axis. It is important to raise the amount of velocity from u=0.1 to u=2 in order to get the desired result.

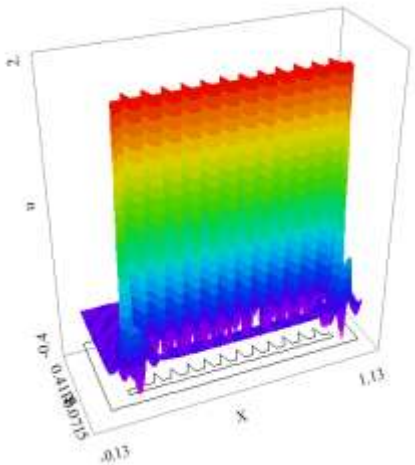

a)Triangular baffles near the bottom wall

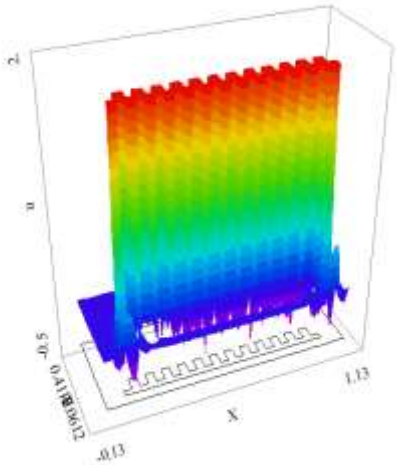

b)rectangular baffles near the bottom wall

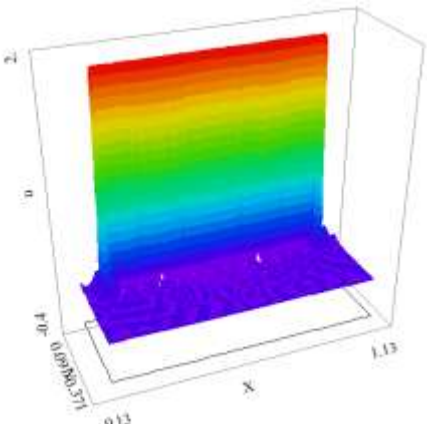

c) Inverse triangular baffles near the top

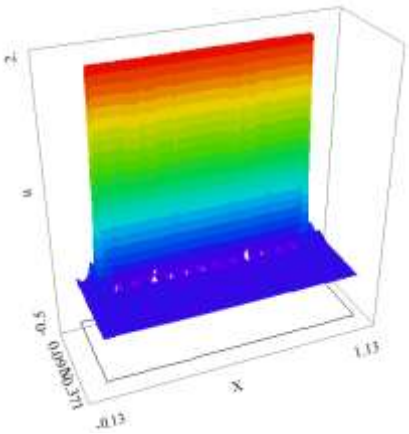

d) Inverse rectangular baffles near the top

Figure 8. *Comparison of velocity (u) changes in different baffles for threated stretching surface.*

As shown in Fig.9, the velocity changes in rectangular and triangular baffles for a similar stretched surface generate a considerable difference in the surface length. The nanofluid velocity in the center of the surface (b-9) in the rectangular baffles above the surface (b-9) is significantly greater than the nanofluid velocity at both the beginning and the end of the surface. The average velocity of nanofluid flow in rectangular baffles is u=0.4 for rectangular baffles and triangular baffles from X=0.2 to X=0.8 for rectangular baffles and triangular baffles.

Figures c-9 and d-9 show how the air velocity changes when the triangular and rectangular baffles are attached to opposing sides of the surface. The velocity in the first baffle achieves its greatest value when operating in triangular baffle mode at X=0. Despite the fact that the entire amount of value is 21, the value of velocity in the x-direction for the first baffle in the case of rectangular baffles is 1.3 (m/s) despite the fact that the total amount of value is 21. Between the X=0.2 and X=0.8, there is no variation in velocity, and the value of velocity between these two places is equal to zero. In the presence of triangle baffles, the rate of nanofluid flow velocity is larger than the rate of nanofluid flow velocity at rectangular baffles.

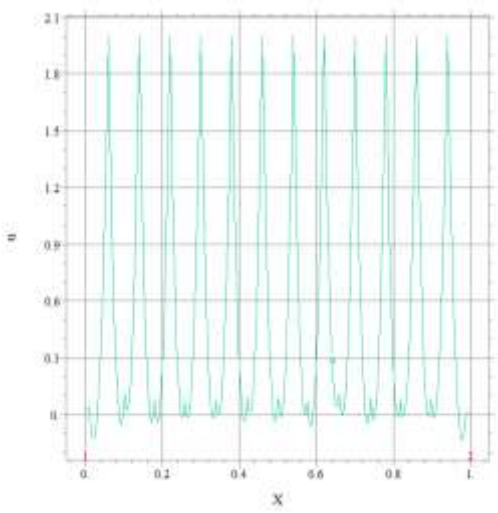

a) Triangular baffles near the bottom wall

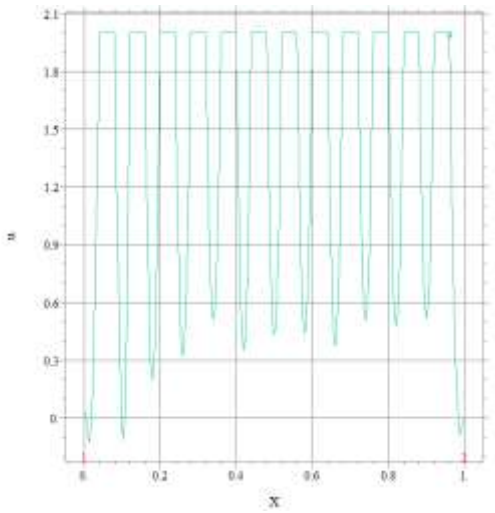

b) rectangular baffles near the bottom wall

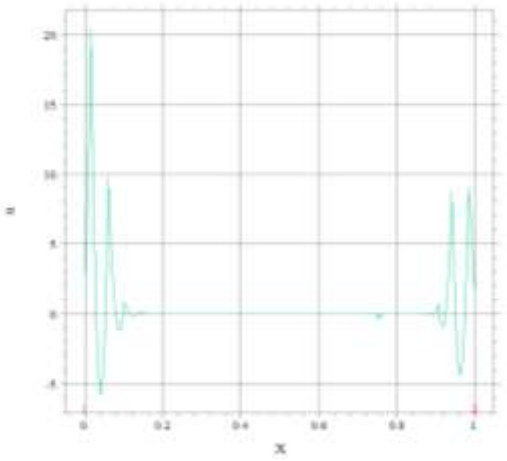

c) Inverse triangular baffles near the top wall.

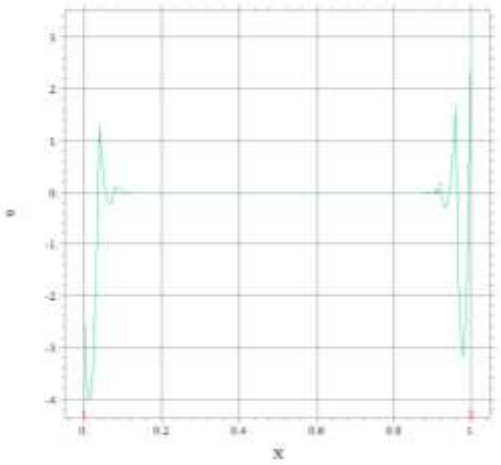

d) Inverse rectangular baffles near the top wall.

Figure 9. *Comparison of velocity (u) changes in in rectangular and triangular baffles for threated stretching surface.*

Fig. 10 shows the temperature change of the nanofluid flow around the triangular and rectangular baffles. The first baffle, depicted in figures a-10 and b-10, includes the nanofluids with the maximum temperature of 34 degrees in the X=0.1 direction. When the water is 30 degrees, the temperature is uniformly spread throughout the liquid's surface.

It can be seen that the temperature of nanofluids rises from X=0 to X=1, as can be seen in the previous figure. The highest temperature is T=30 degrees Celsius, and the lowest temperature is T=20 degrees Celsius. T=30 degrees Celsius is the maximum temperature. The wide variation in temperature is most noticeable in the rectangular and triangular baffles, which are particularly noticeable. According to Table 3, the rectangular baffles exhibit the greatest amount of nanofluid velocity. On the rectangular baffles, the fluid velocity for nanofluid is 19.5 percent greater than the fluid velocity on the other baffles.

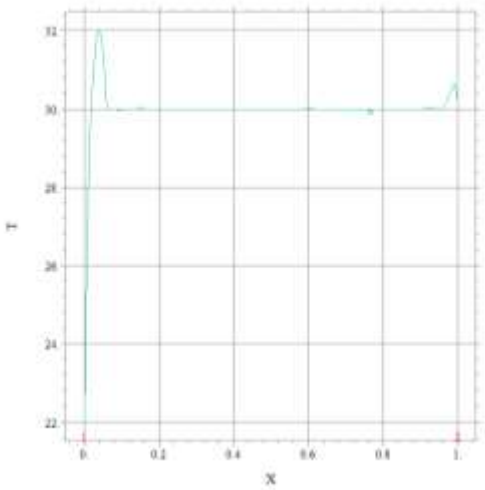

a) Triangular baffles near the bottom wall

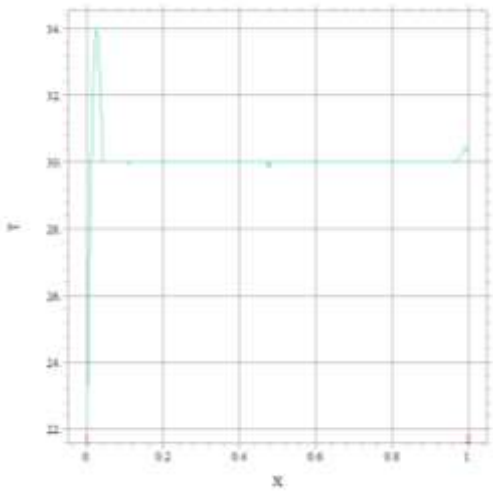

b) rectangular baffles near the bottom wall

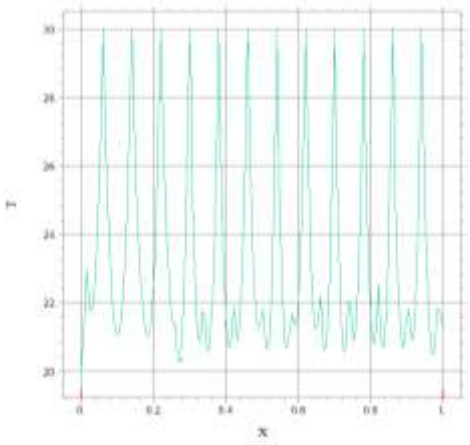

c) Inverse triangular baffles near the top wall

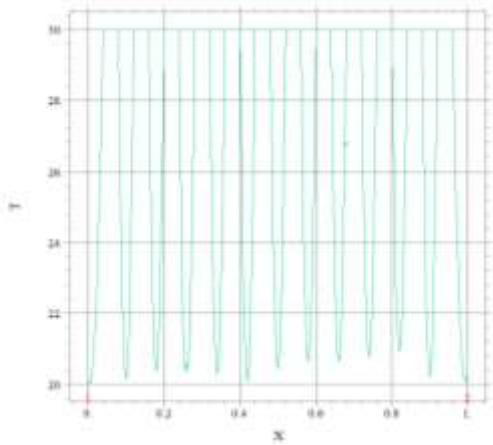

d) Inverse rectangular baffles near the top wall

Figure 10. *Comparison of temperature changes in in rectangular and triangular baffles for threated stretching surface.*

Table 3. *Numerical comparison of nanofluid velocity between different baffles.*

x	$u_{Triangular\ baffle}$	$u_{Rectangular\ baffle}$	$u_{inverse\ rectangular}$	$u_{inverse\ triangular}$
0.0	0	0	0	0
0.2	0.28	1.17	0.34	1.10
0.3	1.55	1.95	1.43	1.54
0.5	0.02	0.42	0.12	0.35
0.8	0.17	1.36	0.19	1.26
1	0	0	0	0

Regarding table 4, the maximum of nanofluid temperature is observed in rectangular and triangular baffles.

The fluid temperature for nanofluid on the rectangular and triangular baffles is 50% bigger than other baffles.

Table 4. *Numerical comparison nanofluid temperature between different baffles.*

x	$T_{Triangular\ baffle}$	$T_{Rectangular\ baffle}$	$T_{inverse\ rectangular}$	$T_{inverse\ triangular}$
0.0	22.07	22.08	20.01	20.01
0.2	27.32	27.26	26.66	22.30
0.3	27.66	27.65	30.01	29.10
0.5	28.53	28.64	21.05	21.18
0.8	29.72	29.72	27.30	21.46
1	30.21	30.16	20.70	20.99

5. CONCLUSION

In this paper, variation of temperature and velocity in the x-direction and the angular velocity of the nanofluid flow through triangular and rectangular baffles are investigated in the existence of a uniform magnetic field. Moreover, the two-scale fractal calculus can model the effect of the Nanoparticles' size and distribution of the flow properties. So, the two-scale transform can approximately convert the fractional calculus into its traditional partner, making the two-scale thermodynamics much more promising.

The innovation of this paper is to investigate parameters of nanofluid flow passing from the different baffles on the stretching surface. The surface is affected by the flow of magnetism. The finite Element Method is selected for solving governing equations.

The summary of the critical results is represented as follows:

- The effect of velocity changes in the x-direction around the baffles has more value than the surrounding space. The amount of flow velocity is reduced by increasing the distance from the surface in the y-direction.

- In the angular velocity of nanofluids in the lower part of the surface, the angular velocity of nanofluids is very high around the baffles and the fluid flow particles orbit around the board at high speeds. The fluid flow velocity in the entire space around the baffles is balanced.

- The volume of nanofluid flow at the beginning of the surface and around the first baffle is very high and has reached its maximum limit. The fluid flow is decreased slightly, and the temperature is balanced around the other edges and the whole surface space as the fluid flow exceeds the baffle.

- In the rectangular baffles above the surface, the nanofluid velocity in the middle of the surface has higher values than at the beginning and end of the surface. At X=0.2 to X=0.8 for rectangular baffles and triangular baffles, the average velocity of nanofluid flow in the rectangular baffles is equal to u=0.4 but the average velocity of nanofluid flow in the triangular baffles is equal to u=0.04. The fluid velocity for nanofluid on the rectangular baffles is 19.5% bigger than other baffles.

- In all the triangular and rectangular baffles on the surface, the highest nanofluids temperature is in the first fin, and its value is equal to 34 degrees in X=0.1. The temperature is balanced all around the surface and has a value of 30 degrees.

- Maximum nanofluid temperature occurs in the rectangular baffles near

the bottom wall. The amount of temperature is 34℃. The maximum temperature for triangular baffles and inverse triangular baffles is 32℃ and 30 ℃ . The fluid temperature for nanofluid on the rectangular and triangular baffles is 50% bigger than other baffles.

DATA AVAILABILITY

The data that support the findings of this study are available on request from the corresponding author. The data are not publicly available due to state restrictions such as privacy or ethical restrictions.

CONFLICT OF INTEREST

The authors declare that they have no conflict of interest.

REFERENCES

1. Maghsoudi, A. A., Soheil, M. J., Darbhenz, A.,"Effect of the Nano Particles in the New Generation of Concretes, SCC", *Int. J. Nanosci. Nanotechnol.,* 6 (2010) 137–143.
2. Ghozatloo, A., Shariaty Niassar, M., Rashidi, A.,"Effect of Functionalization Process on Thermal Conductivity of Graphene Nanofluids", *Int. J. Nanosci. Nanotechnol.,* 13 (2017) 11–18.
3. Gangaiah, T., Saidulu, N., Venkata Lakshmi, A.,"The influence of thermal radiation on mixed convection MHD flow of a casson nanofluid over an exponentially stretching sheet", *Int. J. Nanosci. Nanotechnol.,* 15 2 (2019) 83–98.
4. Peiravi, M. M., Alinejad, J., "3D Numerical Simulation of Fibers Arrangement Effects on Thermal Conductivity of Polymer Matrix Composite", *Mechanics of Advanced Composite Structures, 9* (2022) 59–73.
5. Ji-Huan, H., Mostapha, D. R.,"Insight into the Significance of Hall Current and Joule Heating on the Dynamics of Darcy–Forchheimer Peristaltic Flow of Rabinowitsch Fluid", *Journal of Mathematics*, 2021.
6. Ji-Huan, H., Abd Elazem, N. Y., "Insights into Partial Slips and Temperature Jumps of a Nanofluid Flow over a Stretched or Shrinking Surface", *Energies*, 14 (2021) 1-21.
7. Ji-Huan, H., Moatimid, G. M., Mostapha, D. R.,"Nonlinear instability of two streaming-superposed magnetic Reiner-Rivlin Fluids by He-Laplace method", *Journal of Electroanalytical Chemistry*, 895 (2021).
8. Peiravi, M. M., Alinejad, J., "Hybrid Conduction, Convection and Radiation Heat Transfer Simulation in A Channel with Rectangular Cylinder", *Journal of Thermal Analysis and Calorimetry*, 140 (2019) 2733-2747.
9. Araban, H. P., Alinejad, J., Peiravi, M. M., "Entropy generation and hybrid fluid-solid-fluid heat transfer in 3D multi-floors enclosure", *International Journal of Exergy*, 37 (2022) 337-357.
10. Peiravi, M. M., Alinejad, J., "Nano Particles Distribution Characteristics in Multi-Phase Heat Transfer between 3D Cubical Enclosures Mounted Obstacles", *Alexandria Engineering Journal*, 60 (2021) 5025-5038.
11. Ramya, D., Rao, J. A., Shravani, I., "Numerical Simulation of MHD Boundary Layer Stagnation Flow of Nanofluid over a Stretching Sheet with Slip and Convective Boundary Conditions", *Journal Of Nanotechnology*, 16 (2020) 103-115.
12. Peiravi, M. M., Alinejad, J.,"Numerical analysis of secondary droplets characteristics due to drop impacting on 3d cylinders considering dynamic contact angle",*Meccanica*, 55 (2020) 1975–2002.
13. Ramya, D., Rao, J. A., & Shravani, I.,"Numerical Simulation of MHD Boundary Layer Stagnation Flow of Nanofluid over a Stretching Sheet with Slip and Convective Boundary Conditions", *International Journal of Nanoscience and Nanotechnology*, 16 (2020) 103-115.
14. Gangaiah, T., Saidulu, N., Venkata Lakshmi, A., "The Influence of Thermal Radiation on Mixed Convection MHD Flow of a Casson Nanofluid over an Exponentially Stretching Sheet", *International Journal of Nanoscience and Nanotechnology*, 15 (2019) 83-98.
15. Ghozatloo, A., Shariaty Niassar, M., Rashidi, A.,"Effect of functionalization process on thermal conductivity of graphene nanofluids", *International Journal of Nanoscience and Nanotechnology,* 13 (2017) 11-18.
16. Pushpa, B. V., Sankar, M., Mebarek-Oudina, F., "Buoyant Convective Flow and Heat Dissipation of Cu–H2O Nano liquids in an Annulus Through a Thin Baffle", *Journal of Nanofluids*, 10 (2021) 292-304.
17. Shafiq, A., Mebarek-Oudina, F., Sindhu, N. T., Abidi, A., "A study of dual stratification on stagnation point Walters' B nanofluid flow via radiative Riga plate: a statistical approach", *The European Physical Journal Plus*, 136 (2021).
18. Swain, K., Mebarek-Oudina, F., Abo-Dahab, S.M., "Influence of MWCNT/Fe3O4 hybrid nanoparticles on an exponentially porous shrinking sheet with chemical reaction and slip boundary conditions", *J Therm Anal Calorim,* 147 (2022) 1561–1570.

19. Mebarek-Oudina, F., Fares, R., Aissa, A., Lewis, R.W., Abu-Hamdehe, N. H., "Entropy and convection effect on magnetized hybrid nano-liquid flow inside a trapezoidal cavity with zigzagged wall", *International Communications in Heat and Mass Transfer*, 125 (2021).
20. Dadheech, P. K., Agrawal, P., Mebarek-Oudina, F., Abu-Hamdeh, N. H., Sharma, A., "Comparative Heat Transfer Analysis of MoS2/C2H6O2 and SiO2-MoS2/C2H6O2 Nanofluids with Natural Convection and Inclined Magnetic Field", *Journal of Nanofluids*, 9 (2020) 161-167.
21. Marzougui, S., Mebarek-Oudina, F., Magherbi, M., Mchirgui, A.,"Entropy generation and heat transport of Cu–water nanoliquid in porous lid-driven cavity through magnetic field", *International Journal of Numerical Methods for Heat & Fluid Flow*, (2021).
22. Ji-Huan, H., Na, Q., Chun-Hui, H., "Solitary waves travelling along an unsmooth boundary", *Results in Physics*, 24 (2021).
23. Ji-Huan, H., Wei-Fan, H., Chun-Hui, H., Saeed, T., Hayat, T., "variational approach to fractal solitary waves", *Fractals*, 29 (2021).
24. Jalili, B., Sadighi, S., Jalili, P., Ganji, D. D., "Characteristics of ferrofluid flow over a stretching sheet with suction and injection", *Case Studies in Thermal Engineering*, 14 (2019).
25. Brinkman, H.C., "The viscosity of concentrated suspensions and solutions", *J. Chem. Phys.*, 20 (1952) 571-571.
26. Bourantas, G.C., Loukopoulos, V.C., "MHD natural-convection flow in an inclined square enclosure filled with a micropolar-nanofluid", *Int. J. Heat Mass Transfer*, 79 (2014) 930–944.
27. Khan, U., Ahmed, N., Mohyud-Din, S. T., "Numerical investigation for three dimensional squeezing flow of nanofluid in a rotating channel with lower stretching wall Suspended by carbon nanotubes", *Appl. Therm. Eng*, 113 (2017) 1107–1117.